







Fiber Optic Current Meter for IIoT in Power Grid

Valentina Temkina¹ , Andrey Medvedev¹ ,
Alexey Mayzel¹ , and Alexander Mokeev² 

¹ Peter the Great St. Petersburg Polytechnic University (SPbPU),
Polytechnicheskaya, 29, St. Petersburg 195251, Russia
temkina.vs@edu.spbstu.ru, medvedev@rphf.spbstu.ru,
amayzel@gmail.com

² OOO 'Electro', Nauki pr. 17/6, St. Petersburg 195220, Russia
mokeeff@mail.ru

Abstract. The article is focused on the fiber optic current meter with FPGA-based data processing. The sensor element operation is based on the Faraday effect which occurs in the Spun optical fiber twisted around electric wire. The demodulation method used to process the sensor signal is the joint measuring of the first and second harmonics of the modulation signal and the processing of their ratio. It is widely known for fiber optic gyroscopes and traditionally is performed in the analog form, fully or partially. This leads to errors related to instability of the analog elements, limited operating range of the device etc. We managed to combine the optical sensor circuit with NI technologies to develop and implement digital data processing algorithms, exclude sources of errors from the optical device circuit. We used a scalable NI RIO architecture, LabVIEW FPGA and LabVIEW Real-Time to implement every step in optical sensing of electric current: modulation forming, response measuring, inline processing and analog/IEC 61850 output providing, comparing performance of high-end and low-cost RIO devices.

Keywords: Fiber optic current meter · Faraday effect · Fiber optic sensor
Spun fiber

1 Introduction

There is a century-old approach to measure high current values (from hundreds of amperes to hundreds of thousands of amperes) by transforming it to the appropriate for metrology equipment levels using inductive coupling. The devices traditionally used for this purpose are called measuring (or primary) transformers. This solution worked just fine for pre-digital era, but even then, it had some well-known significant limitations in measuring transient currents, especially in emergency shortage or significant overload, which caused protection malfunction or false triggering. After moving the power grid automation and protection systems to all-digital base, it appeared that a use of secondary transducers is needed to convert an output of measuring transformers to ADC input levels.

It was an industry demand to build a solution that performs electrical measurements using a physical process other than inductive transformation. In early 2000s, the pioneer in this field NXT Phase delivered the first commercial optical current transformer. Later there were several enhancements of this technology made by market players, bringing the optical current sensing to its modern look. Nowadays these are complex devices, ready to work in both analog environment and such-called digital substations, operating in IEC 61850 standard.

Despite a couple of decades of evolution, the technology is not flawless. One of the main challenges here is cost reduction for the product. One of the most expensive components of the optical current transformer is an optical delay line, which is a long (several hundreds of meters) polarization maintaining (PM) optic fiber. The exclusion of this delay line could make optical sensing far more competitive, but requires deep changes in physical approach, optical scheme and digital processing algorithms.

Another important challenge that we must solve is to improve the algorithm of data processing. Traditionally, signal processing is performed fully or partially in the analog form, but this leads to errors related to instability of analog elements, limitation of the operating range of the device etc. Therefore, in order to eliminate undesirable effects and improve the accuracy of the sensor, we realized the demodulation method completely in digital form.

We at Peter the Great Polytechnic University have made a theoretical study of the design of such solution and have used National Instruments (NI) technologies to implement it in the hardware.

2 Current Meter Optical Scheme

2.1 Description

The scheme of the current sensor is shown in Fig. 1.

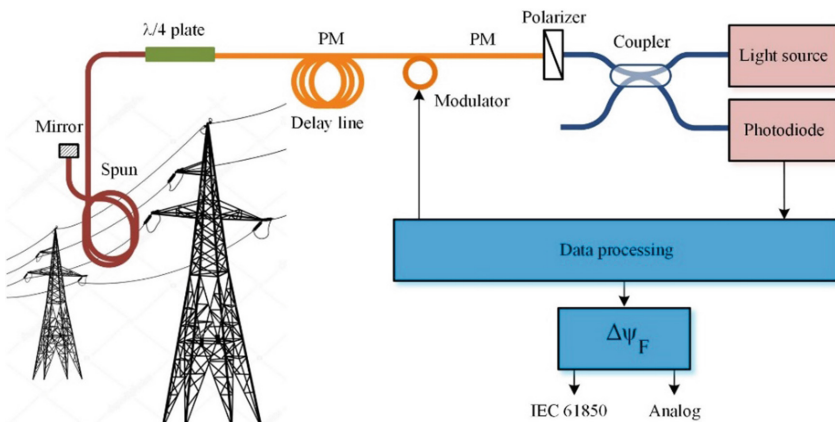


Fig. 1. Scheme of fiber-optic current meter.

The main components of the optical scheme of the meter are:

- light source;
- phase modulator made of a PM optical fiber coiled on a PZT cylinder;
- fiber delay line;
- fiber quarter wave plate;
- sensing element made of the Spun optical fiber;
- mirror;
- polarizer;
- photodiode;
- data processing unit.

The meter uses additional harmonic phase modulation:

$$\Delta \psi_M(t) = \psi_m \cdot \cos(2\pi f_M t) \quad (1)$$

where the modulation frequency $f_M = 40.1$ kHz corresponds to the piezoceramics resonant frequency. In addition, the meter uses digital phase detection, constructed according to the scheme of analysis of the ratio of harmonics of the modulation frequency [1].

2.2 Circuit Operation Principle

The optical wave passes through the fiber optic coupler, the polarizer and goes to the phase modulator. The polarizer axis is at 45° to the own polarization axes of the PM fiber of the modulator. Optical radiation propagates through the modulator in the form of two light waves with orthogonal linear polarizations. Then the light passes through the delay line whose length is determined by the frequency of the modulation signal. It provides such a lag between the light waves propagating in the forward and backward directions so that during the propagation of the wave from the phase modulator to the mirror and back, the phase of the modulating voltage changes by 180° . The phase plate, whose axes are oriented at the angle of 45° to the own axes of the supply path, converts linearly polarized modes to the circularly polarized modes. They propagate at different speeds in the sensitive Spun fiber, which is coiled around the wire with the current to be measured. In this case, a phase shift proportional to the current in the wire arises between them:

$$\Delta \psi_F = 2VN I \quad (2)$$

where V is the Verde constant for the fiber, N is the number of fiber turns around the conductor with current I [2].

The light wave, reflected from the mirror, propagates in the opposite direction. With a repeated pass of the phase plate, the circularly polarized modes are again transformed into linearly polarized modes. As a result, only the Faraday phase shift, connected with the measured electric current, is conserved. Linearly polarized modes, passing through the polarizer, interfere, and then the interference signal through the splitter goes to the photodiode.

3 Signal Demodulation Method

The optical power of the signal at the input of the photodiode is the sum of the harmonics of the modulation frequency:

$$P(\Delta\psi_F, t) = P_0[1 + \cos(\Delta\psi_F + \psi_m \cos(2\pi f_M t))] = P_0[1 + \cos(\Delta\psi_F) \cos(\psi_m \cos(2\pi f_M t)) - \sin(\Delta\psi_F) \sin(\psi_m \cos(2\pi f_M t))] \quad (3)$$

Using expansion in terms of Bessel functions gives

$$P(\Delta\psi_F, t) = P_0 + P_0 \cos(\Delta\psi_F) \cdot [J_0(\psi_m) + 2J_2(\psi_m) \cos(4\pi f_M t) + 2J_4(\psi_m) \cos(8\pi f_M t) + \dots] + P_0 \sin(\Delta\psi_F) [2J_1(\psi_m) \sin(2\pi f_M t) + 2J_3(\psi_m) \sin(6\pi f_M t) + \dots] \quad (4)$$

wherein $J_k(\psi_m)$ are Bessel functions of the first kind of the k -th order.

It can be seen from Eq. (4) that the amplitudes of the harmonics depend on the optical power P_0 and on the values of the Bessel functions. Even harmonics are proportional to $\cos(\Delta\psi_F)$, and odd ones are proportional to $\sin(\Delta\psi_F)$. In the state of rest, the detected signal consists of even harmonics of the modulation frequency, and in the presence of a magnetic field created by an electric current, odd harmonics of the modulation frequency also appear.

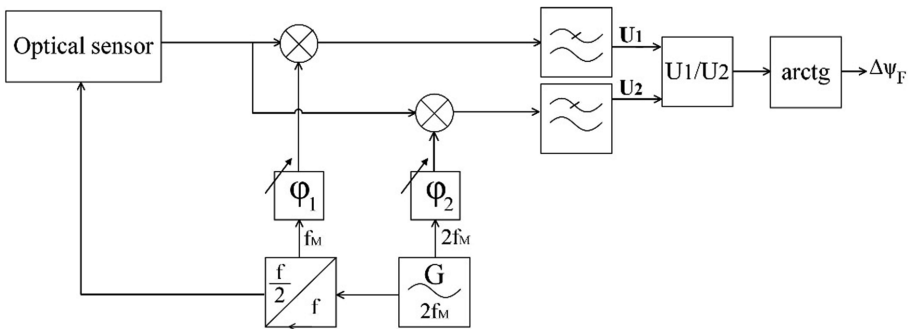


Fig. 2. Block diagram of signal demodulation method

The demodulation method used to process the sensor signal and is widely known in fiber optic gyroscopes is the joint recording of the first and second harmonics of the modulation frequency and the analysis of their ratio (see Fig. 2).

We used synchronous detection of the photodiode’s output voltage at frequencies f_M and $2f_M$ to obtain two quadrature signals:

$$U_1 \sim \sin(\Delta\psi_F) \cdot J_1(\psi_m) \cdot \cos(\Delta\phi_1) \quad (5)$$

$$U_2 \sim \cos(\Delta\psi_F) \cdot J_2(\psi_m) \cdot \cos(\Delta\phi_2) \tag{6}$$

where $\Delta\phi_1$ and $\Delta\phi_2$ – phase shifts between the corresponding reference signals and the detected frequency components. We achieved $\cos(\Delta\phi_1) = \cos(\Delta\phi_2) = 1$ by adjusting the phase shifters. The amplitude of the phase modulation should be chosen so that Bessel functions $J_1(\psi_m)$ and $J_2(\psi_m)$ are equal and maximum at the same time.

As a result, the output signal of the fiber optic current sensor is given by the following formula:

$$\Delta\psi_F = \arctg \frac{U_1}{U_2} = \arctg \left[\frac{J_1(\psi_m)}{J_2(\psi_m)} \operatorname{tg}(\Delta\psi_F) \right] \tag{7}$$

4 Compensation of the Result Dependence on the Modulation Amplitude

It is clear from the Eq. (7) that the amplitude of the phase modulation affects the result of the demodulation. Therefore, it is necessary (a) to select optimal phase modulation amplitude and (b) to compensate demodulation errors occurring due uncontrolled amplitude variation.

Optimal amplitude was chosen based on the following two criteria:

- the first U_1 and second U_2 harmonics of the modulation frequency must be maximal and equal;
- optimal amplitude should correspond to minimum errors arising due amplitude variation.

We choose optimal amplitude $\psi_{m0} = 2.629874$ radians that corresponds to the minimum amplitude value giving $J_1(\psi_{m0}) = J_2(\psi_{m0})$.

If the modulation amplitude deviates from the optimal operating value, the ratio of the Bessel functions in Eq. (7) becomes different from 1. Hence, an error arises when calculating the arctangent. Therefore, we introduced compensation, thanks to which Bessel functions ratio in Eq. (7) is maintained equal to one in a certain range of amplitudes. In order to take into account the effect of the deviation of the modulation amplitude, it is convenient to use the ratio of the second and fourth harmonics of the photodiode’s output signal

$$\frac{U_2}{U_4} = J_2(\psi_m)/J_4(\psi_m) \tag{8}$$

The Eq. (7) with compensation has the following form

$$\Delta\psi_F = \arctg \left[\frac{U_1}{U_2} \cdot \left\{ 1 + k_1 \left(\frac{U_2}{U_4} - 5.30176 \right) + k_2 \left(\frac{U_2}{U_4} - 5.30176 \right)^2 + k_3 \left(\frac{U_2}{U_4} - 5.30176 \right)^3 \right\} \right]$$

$$= \arctg \left[\frac{J_1(\psi_m)}{J_2(\psi_m)} \cdot g(\psi_m) \cdot \text{tg}(\Delta\psi_F) \right], \tag{9}$$

where

$$g(\psi_m) = 1 + k_1 \left(\frac{J_2(\psi_m)}{J_4(\psi_m)} - 5.30176 \right) + k_2 \left(\frac{J_2(\psi_m)}{J_4(\psi_m)} - 5.30176 \right)^2 + k_3 \left(\frac{J_2(\psi_m)}{J_4(\psi_m)} - 5.30176 \right)^3 \tag{10}$$

is the error correction function and $\frac{J_2(\psi_{m0})}{J_4(\psi_{m0})} = 5.30176$ for optimal phase modulation amplitude.

Modified block diagram of signal demodulation looks like in Fig. 3.

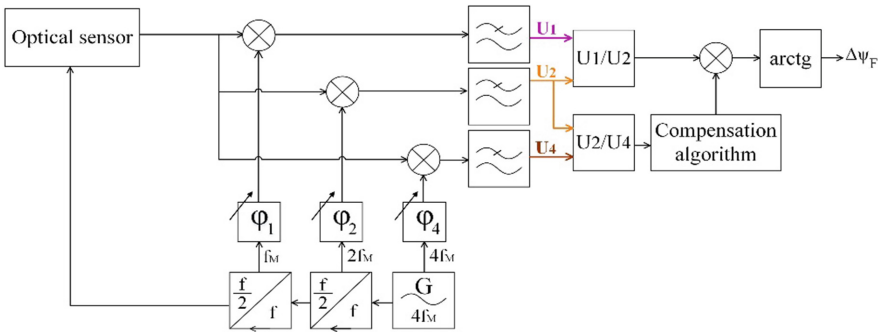


Fig. 3. Block diagram of signal demodulation with compensation

5 Implementation

There were three major cycles of development of our solution: PC-based modeling, first prototype and industrial prototype. From the very beginning our team started modeling the processing using LabVIEW graphical tools. First step model was developed in floating-point math with both calculated and measured signal waveforms. It showed the predicted results of basic demodulation and demodulation with compensation.

The modeling code was built with consideration of future conversion to FPGA-applicable integer and fixed-point math. Thus, there was no need to write completely new code for implementation in a prototype (as shown in Fig. 4).

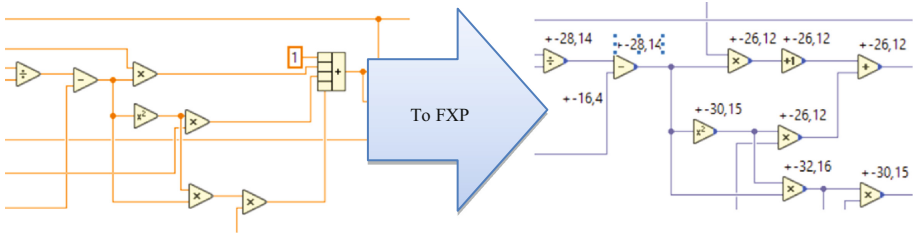


Fig. 4. An example of code transformation from host-based floating-point (left) to FPGA fixed-point (right). The code shown implements the compensation.

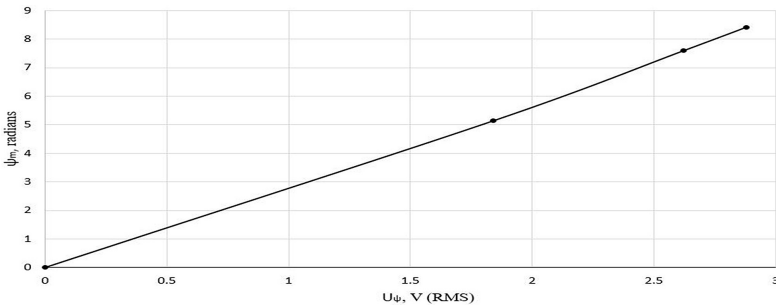


Fig. 5. Calibration of the phase modulator

When modeling in the LabVIEW program environment, the coefficients k_1 , k_2 and k_3 were chosen so that the function $g(\psi_m)$ in Eq. (9) was as close as possible to one in the neighborhood of optimal amplitude ψ_{m0} . Figure 6 presents simulation results without compensation, floating-point compensation model, fixed-point FPGA implementation, as well as experimental data. Thus, as a result of compensation, within the range of amplitudes of $\pm 6\%$ from the optimal amplitude ψ_{m0} the error was within the limits of $\pm 0.1\%$ with the coefficients chosen in the program. Less variations of ψ_m gives smaller values of errors up to $\pm 0.0001\%$.

Before starting the experiments, we calibrated phase modulator used in the sensor. Calibration was carried out in absence of any measured signal by measuring modulation amplitudes corresponding to zero values of Bessel functions of the first kind of even orders. As a result, a calibration curve was obtained for a modulator fed at resonance frequency (see Fig. 5). From this curve follows that the optimal modulation voltage corresponding to $\psi_{m0} = 2.629874$ is $U_{\psi 0} = 0.9163$ V.

The first prototype was implemented on entry-level hardware unit of National Instruments RIO platform named myRIO [3]. It's a low-cost device designed for educational purposes with limited IO lines and FPGA resources. With all these limitations this hardware allowed our team to build a functional prototype with fully synchronous inline FPGA processing, Real-Time OS supervision and control and desktop GUI. We managed to run verification tests on our theoretical research and selected system architecture.

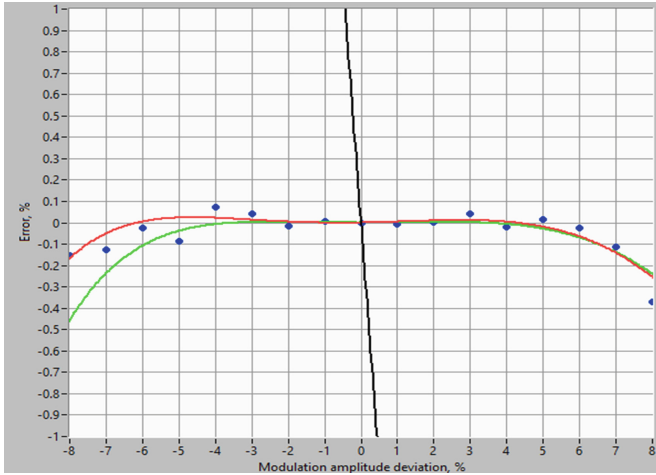


Fig. 6. Error RMS vs Modulation amplitude deviation graph. Black – uncompensated. Green – floating-point compensation model. Red – fixed-point FPGA implementation. Blue – experimental data. (Color figure online)

NI myRIO is equipped with 4 analog inputs and 2 analog outputs, which allowed us to generate a modulating signal, register the signal of the photodetector and generate an analog signal for feeding the comparison instrument. However, an inexpensive, compact controller designed primarily for educational purposes can generate an output signal with a sampling frequency of a maximum of 345 kHz and a resolution of 12 bits, that is, 8 points for a modulation cycle of 40 kHz and 4 points for a second harmonic of the modulation frequency. In this regard, the maximum accuracy that was achieved by the comparison instrument was about 1% in amplitude and half degree in phase. To increase the sampling frequency and bit capacity, external ADCs and DACs were used together with myRIO, which also increased the accuracy of the sensor analog output readings.

The front panel of the signal-processing program is shown in Fig. 7. The graphs at the upper part of the panel show the first (blue) and second (red) harmonics of the modulation frequency, as well as the photodiode’s signal (green). On the bottom of the panel left graph indicates the error correction function $g(\psi_m) - 1$, zero value corresponding to phase modulation amplitude equal to ψ_{m0} and $g(\psi_m) = 1$. The analog signal used for measuring comparator instrument feeding is shown at the bottom right side of the panel.

It was an easiest transition between alpha prototype and industrial prototype because of keeping NI RIO platform. The NI System-On-Module (SOM) sbRIO-9651 was selected. NI SOM is an example of the same FPGA-based RIO architecture [4]. This allowed us to migrate code completely from alpha prototype, changing only IO numbers. The bigger FPGA and larger number of DIO lines opened the possibilities to achieve a faster timing, finer tuning and wider process control. The front panel of the signal-processing program using NI SOM are presented in Fig. 8.

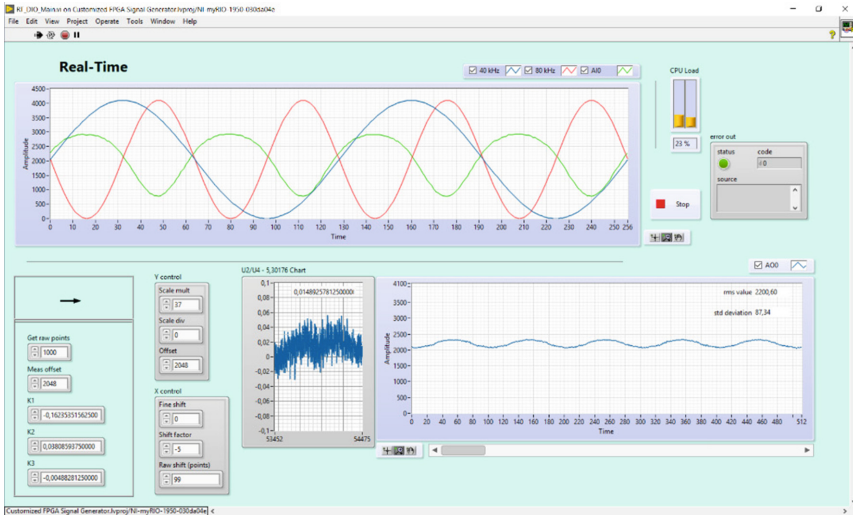


Fig. 7. The front panel of the signal-processing program for the current meter when using NI myRIO with external ADCs and DACs (Color figure online)

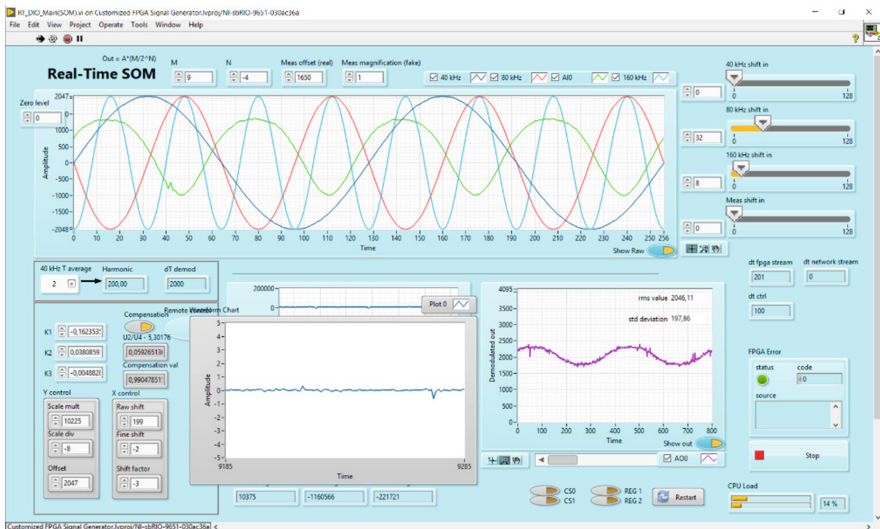


Fig. 8. The front panel of the signal-processing program for the current meter when using NI SOM.

In electrical metrology only specially designed high precision analog measuring comparator instruments are certified to calibrate sensors. So we used output digit to analog converter (DAC) to feed this comparator instrument and NI ready to use Toolkit to obtain standard IEC 61850 signal for future applications.

6 Conclusions

In our paper we had shown that digital processing can be applied to fiber optic current sensing replacing traditional analog demodulation methods with benefits of inline error correction. It allowed us to eliminate errors induced by instability of the analog elements, limited operating range of the device, modulation amplitude deviations within the range of $\pm 2\%$ from the optimum value. The proposed method of error correction demonstrated potential accuracy of such devices of about 0.0001% that is compliant to the modern metrology certification demands to the power grid devices. The results of PC-based modeling showed a good level of correlation with experimental data acquired using NI RIO hardware with fully synchronous onboard FPGA control and processing.

Acknowledgments. The work was done under financial support of Ministry of Education and Science of the Russian Federation in terms of FTP “Research and development on priority trends of Russian scientific-technological complex evolution in 2014–2020 years” (agreement # 14.578.21.0211, agreement unique identifier RFMEFI57816X0211).

References

1. Berg, R.A., Lefevre, H.C., Shaw, H.J.: An overview of fiber-optic gyroscopes. *J. Lightwave Technol.* **2**, 91–107 (1984)
2. Bohnert, K., Gabus, P., Nehring, J., Brandle, H.: Temperature and vibration insensitive fiber-optic current sensor. *J. Lightwave Technol.* **20**, 267 (2002)
3. NI myRIO. <http://www.ni.com/myrio/>. Accessed 29 May 2018
4. CompactRIO System on Module. <http://www.ni.com/en-us/shop/select/compactrio-system-on-module>. Accessed 29 May 2018